Supplementary Information

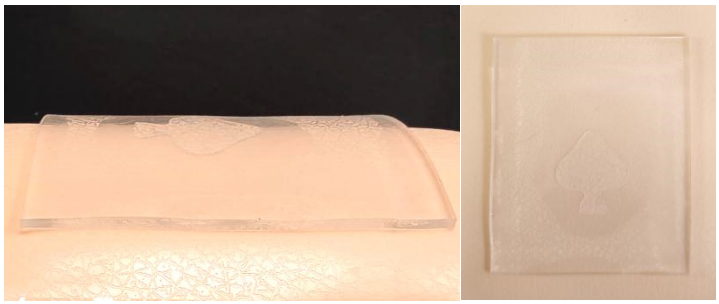

Figure S1: Photographs of the flexible PDMS waveguide.

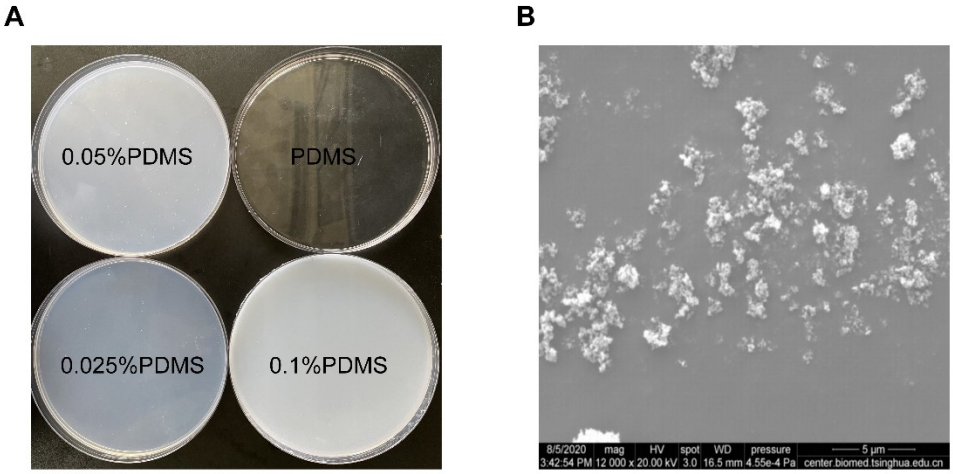

Figure S2: Characterization of TiO_2 NP-PDMS composite waveguide materials. (A) Optical photographs of PDMS samples with varying concentrations of TiO_2 nanoparticles, showing the change in appearance from transparent to milky white. (B) The SEM image shows well-dispersed TiO_2 nanoparticles without significant agglomeration.

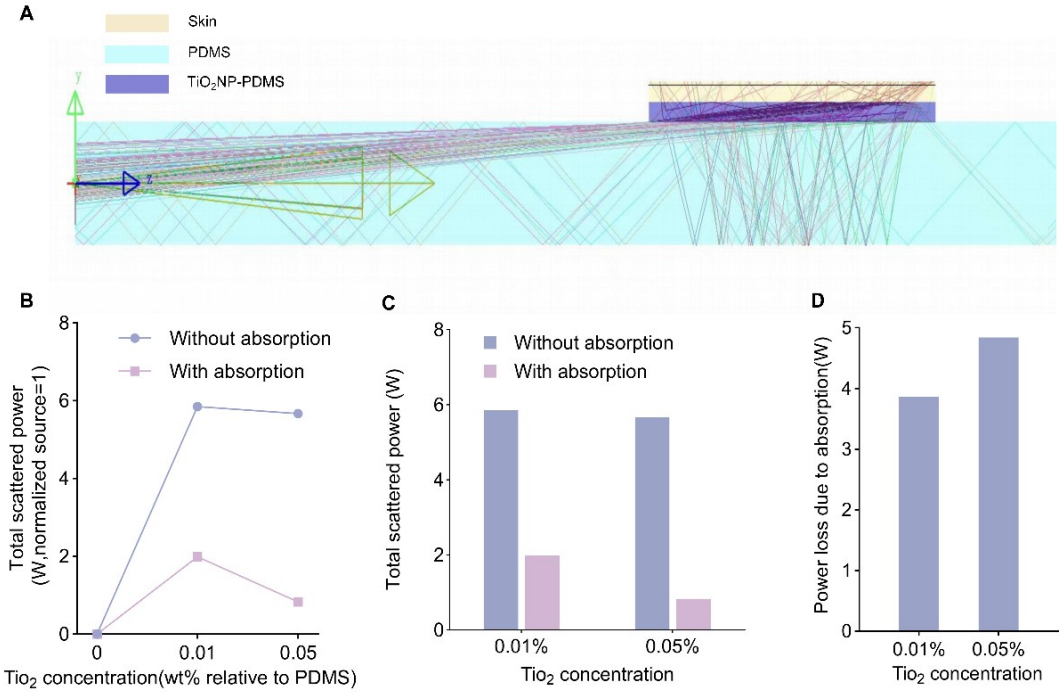

Figure S3: Optical ray-tracing simulations of the composite waveguide. (A) Cross-sectional ray-tracing schematic showing the light extraction from the PDMS guiding layer into the skin via the TiO_2NP-PDMS scattering layer. (B) Simulated effective optical output versus TiO_2NP concentration, exhibiting an optimal peak at 0.01 wt%. (C) Effect of intrinsic material absorption on the simulated scattered output. (D) Calculated absorption penalty at 0.01 wt% and 0.05 wt%, highlighting the severe optical loss induced by multiple scattering at high concentrations.

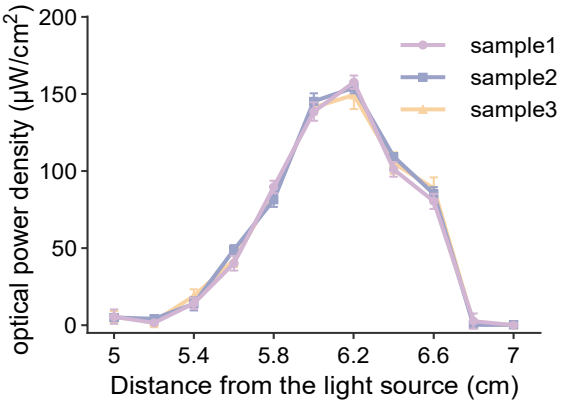

Figure S4: TiO_2NP-PDMS Reproducibility.

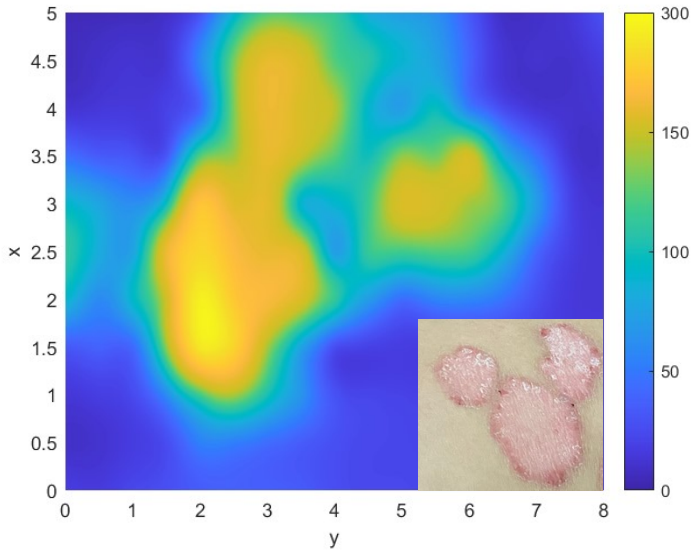

Figure S5: Spatial light intensity distribution map at 308 nm.

Figure S6: UV Irradiation Simulation Using a Miniaturized Setup.

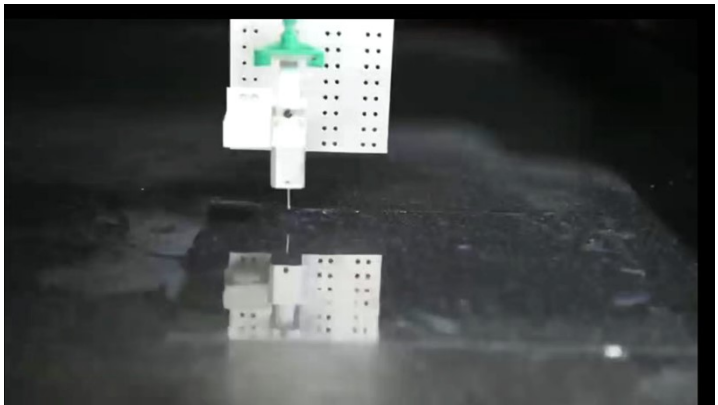

Figure S7: 3D printing process of the TiO_2NP-PDMS composite patch.

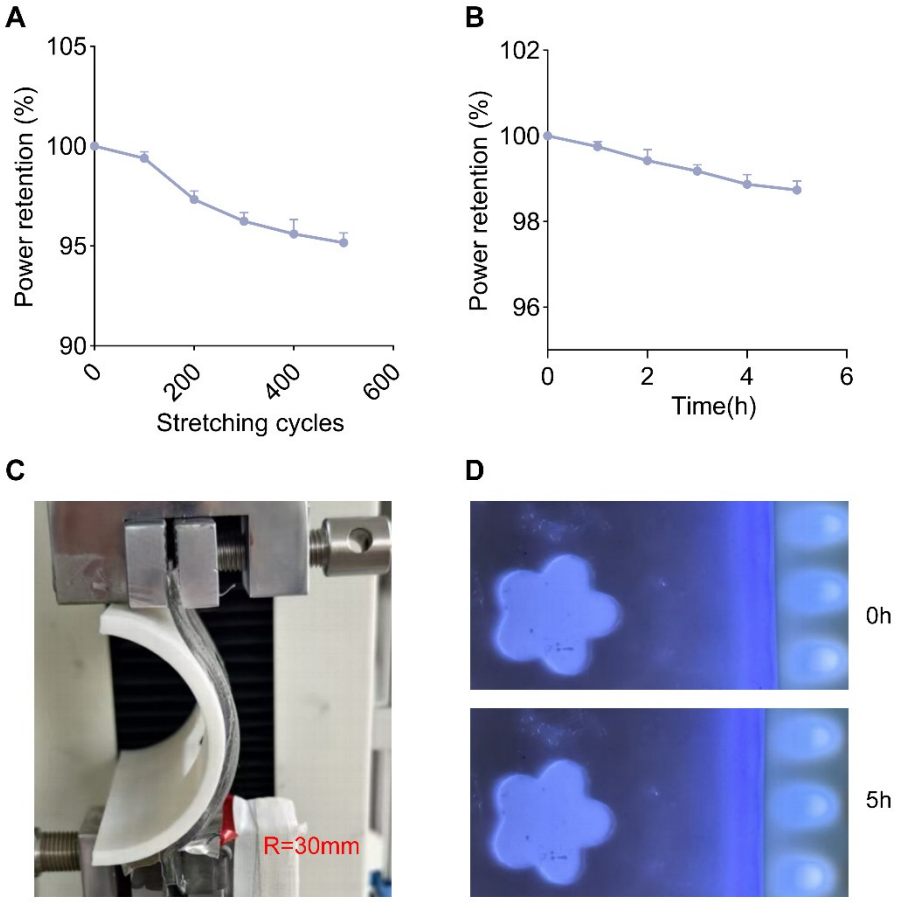

Figure S8: (A) Power retention during 500 mechanical stretching cycles. (B) Power retention during 5 hours of continuous immersion in artificial sweat. (C) Corresponding photograph of the stretching experimental setup showing the patch undergoing testing. (D) Corresponding images of the patch under 308 nm UV

irradiation before (0 h) and after (5 h) the 5-hour immersion test.

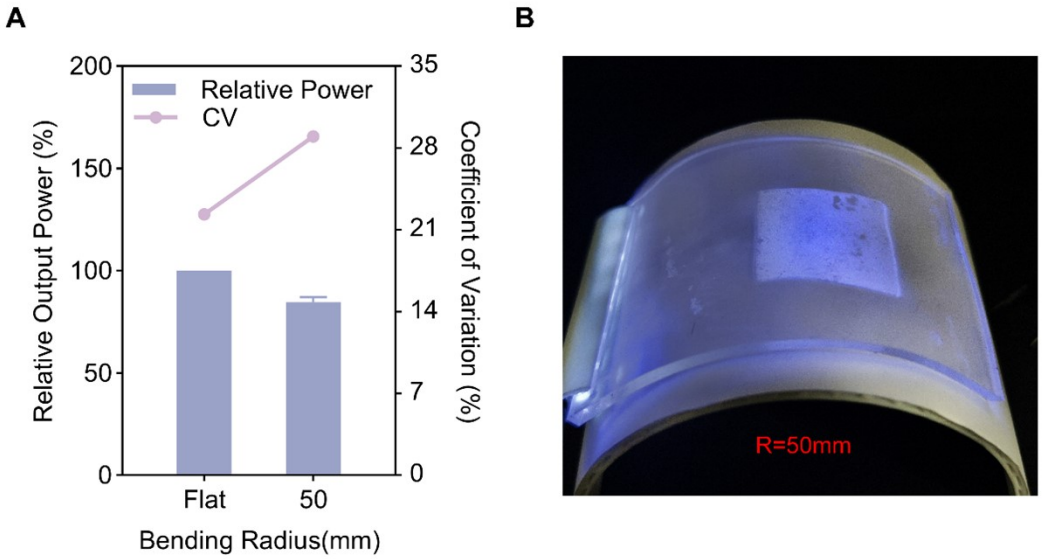

Figure S9: Optical performance stability under bending. (A) Relative output power and coefficient of variation (CV) for flat and curved (R = 50 mm) conditions. (B) Photograph of the illuminated flexible patch on a 50 mm radius surface. Error bars: standard deviation (n=3).

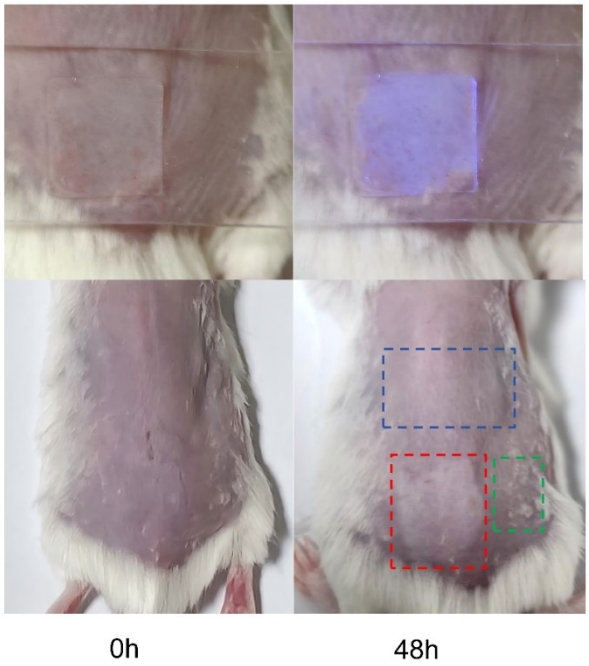

Figure S10. In vivo application of the patterned waveguide patch.

Upper row: Photographs of the patch applied on the mouse back under natural light (left) and 308 nm UV light (right), demonstrating targeted light delivery.

Lower row: Skinappearance at 0 and 48 h post-treatment. Dashed boxes (at 48 h) indicate regions for TEWL measurement: normal unexposed skin (blue), 308 nm-treated lesions (red), and patch-protected adjacent healthy skin (green).

Table S1: Comparison of key performance parameters between the proposed flexible light-guiding patch and recently reported wearable or commercial phototherapy devices.

Reference	Device Architecture	Operating Wavelength (nm)	Output Power Density (mW/cm²)	Spatial Uniformity (CV%)	Skin-contact Safety	Temperature Rise(ΔT, °C)
Ullahet al., 2023[1]	Flexible smart bandage	265 (UVC)	~0.1(Calculated)	Not reported[a]	Biocompatible	~0
Lee et al., 2023[2]	Prototype wearable LED	285 (UVB)	Not reported [b]	Not reported[a]	Mild reactions (11.8% dropout)	Not reported
Horiz.et al., 2026[3]	Flexible OLED patch	630 (Red)	5	Not reported[a]	Biocompatible	< 4
He et al., 2025[4]	Flexible OLED patch	308 (UVB)	16–20	Not applicable[c]	Direct contact unfeasible	Not applicable
Shi et al., 2013[5]	Commercial rigid laser	308 (UVB)	50	Not applicable[c]	Direct contact unfeasible	Not applicable
This Work	Flexible light-guiding patch	308 (UVB)	~0.2	21%	Excellent (Direct attachable)	< 4

CV: Coefficient of Variation, Δ**T**: Temperature rise.

[a] These parameters were not explicitly reported, as these studies primarily focused on material stretchability or basic in-vitro demonstrations rather than clinical-grade optical precision.

[b] The original paper reported a total therapeutic dose (7.8 mJ/cm²), but continuous output power density was omitted.

[c] Commercial rigid 308 nm devices require a strict working distance (typically non-contact) due to high local power, making direct skin-contact metrics (uniformity, contact temp rise) fundamentally unmeasurable or not applicable.

References

1 I. Ullah, M. Wagih, Y. Sun, Y. Li, K. Hajdu, R. Courson, C. Dreanno, E. Prado, A. Komolafe, N. R. Harris, N. M. White and S. Beeby, *IEEE Transactions on Biomedical Circuits and Systems*, 2023, **17**, 900–915.

2 H. J. Lee, S. Yoo, J. K. Hong, J. S. Ahn, E. Lee, H. Moon, S. Koo, T. Kim, J. Park and I.-Y. Yoon, *Eur J Clin Nutr*, 2023, **77**, 342–347.

3 H. Yeon, S. Yu, M. Lee, S. Kim, Y. Park, H.-R. Choi, W. I. Choi, C.-H. Huh, Y. Jeon, C.-S. Park, D. Sung and K. C. Choi, *Mater. Horiz.*, DOI:10.1039/D5MH02129D.

4 J. He, J. Xiang, D. Feng, L. Wang, X. Li, Y. Chen, H. Wang and Y. Xiao, *Photodermatology, Photoimmunology & Photomedicine*, 2025, **41**, e70059.

5 Q. Shi, K. Li, J. Fu, Y. Wang, C. Ma, Q. Li, C. Li and T. Gao, *Photoderm Photoimm Photomed*, 2013, **29**, 27–33.